



HAL
open science

Geographic variations in the slope of the $\delta^{2}\text{H}$ – $\delta^{18}\text{O}$ meteoric water line over Europe: A record of increasing continentality

Christophe Lécuyer, Ana-Voica Bojar, Valérie Daux, Serge Legendre

► To cite this version:

Christophe Lécuyer, Ana-Voica Bojar, Valérie Daux, Serge Legendre. Geographic variations in the slope of the $\delta^{2}\text{H}$ – $\delta^{18}\text{O}$ meteoric water line over Europe: A record of increasing continentality. The Geological Society, London, Special Publications, 2021, 507, pp.SP507-2020-68. 10.1144/SP507-2020-68. hal-02897843

HAL Id: hal-02897843

<https://hal.science/hal-02897843>

Submitted on 8 Jul 2021

HAL is a multi-disciplinary open access archive for the deposit and dissemination of scientific research documents, whether they are published or not. The documents may come from teaching and research institutions in France or abroad, or from public or private research centers.

L'archive ouverte pluridisciplinaire **HAL**, est destinée au dépôt et à la diffusion de documents scientifiques de niveau recherche, publiés ou non, émanant des établissements d'enseignement et de recherche français ou étrangers, des laboratoires publics ou privés.

Accepted Manuscript

Geological Society, London, Special Publications

Geographic variations in the slope of the $\delta^2\text{H}$ – $\delta^{18}\text{O}$ meteoric water line over Europe: A record of increasing continentality

Christophe Lécuyer, Ana-Voica Bojar, Valérie Daux & Serge Legendre

DOI: <https://doi.org/10.1144/SP507-2020-68>

Received 30 March 2020

Revised 17 June 2020

Accepted 18 June 2020

© 2020 The Author(s). Published by The Geological Society of London. All rights reserved. For permissions: <http://www.geolsoc.org.uk/permissions>. Publishing disclaimer: www.geolsoc.org.uk/pub_ethics

Supplementary material at <https://doi.org/10.6084/m9.figshare.c.5040647>

When citing this article please include the DOI provided above.

Manuscript version: Accepted Manuscript

This is a PDF of an unedited manuscript that has been accepted for publication. The manuscript will undergo copyediting, typesetting and correction before it is published in its final form. Please note that during the production process errors may be discovered which could affect the content, and all legal disclaimers that apply to the book series pertain.

Although reasonable efforts have been made to obtain all necessary permissions from third parties to include their copyrighted content within this article, their full citation and copyright line may not be present in this Accepted Manuscript version. Before using any content from this article, please refer to the Version of Record once published for full citation and copyright details, as permissions may be required.

Geographic variations in the slope of the $\delta^2\text{H}$ – $\delta^{18}\text{O}$ meteoric water line over Europe: A record of increasing continentality

[Local meteoric water lines over Europe]

Christophe Lécuyer^{1,2,*}, Ana-Voica Bojar^{3,4}, Valérie Daux⁵ & Serge Legendre¹

¹*Laboratoire de Géologie de Lyon, CNRS UMR 5276, Université Claude Bernard Lyon 1, France*

²*Institut Universitaire de France, 103 Boulevard, Saint-Michel, 75005 Paris, France*

³*Department of Geology, Salzburg University, Hellbrunnerstrasse 34, A-5020, Salzburg, Austria*

⁴*Department of Mineralogy, Universalmuseum Joanneum, Weinzöttlstrasse 16, A-8045, Graz, Austria*

⁵*UMR CEA/CNRS/UVSQ 8212, LSCE, Université de Versailles, Saint-Quentin, France*

*Corresponding author (christophe.lecuyer@univ-lyon1.fr)

Abstract: $\delta^2\text{H}$ and $\delta^{18}\text{O}$ values of precipitations follow an empirical linear relationship at the global scale that is called the Global Meteoric Water Line (GMWL) and characterized by a slope of 8. However, Local Meteoric Water Lines (LMWL) may have different slopes S depending on their geographic situation. Monthly $\delta^2\text{H}$ and $\delta^{18}\text{O}$ of precipitation have been compiled from European

IAEA stations. Those data allowed the calculation of the slopes S of the $\delta^2\text{H}-\delta^{18}\text{O}$ LMWL determined for each station. S increases with longitude ϕ from ≈ 5 (Portugal) to ≈ 9 (Russia), they are positively correlated with relative humidity (RH), negatively with temperature, and positively with the mean intra-annual amplitude of temperatures, which is a proxy of continentality. Slopes of 5 to 6, recorded in southwest Europe, reflect mean RH (70 to 75%) and sea surface temperatures ($\approx 25^\circ\text{C}$) of the Central Atlantic Ocean where the main flux of moisture is formed before being transported by the westerlies. In addition, falling water droplets within an air column with a high RH ($> 80\%$) and low temperature are expected to escape sub-cloud evaporation. Therefore, slopes with values close to 9 are considered to reflect isotopic equilibrium conditions during the condensation of water vapour in clouds.

Keywords: meteoric water line, stable isotopes, continentality, water cycle, Europe

Supplementary material: Supplementary Tables 1 and 2 are available at <https://doi.org/xxxx>.

Hydrogen and oxygen stable isotopes fractionate with large magnitude ($\approx 400\%$ for $^2\text{H}/^1\text{H}$ and 50% for $^{18}\text{O}/^{16}\text{O}$) during phase changes and distillation processes in the atmosphere (Craig 1961; Dansgaard 1964; Rozanski *et al.* 1993). Therefore, they have been recognized for decades as powerful natural tracers of the water cycle (Craig 1961; Craig & Gordon 1965; Dansgaard 1964; Rozanski *et al.* 1993; Gat 1996; Gat *et al.* 2001; Rozanski 2005). $\delta^2\text{H}$ and $\delta^{18}\text{O}$ of meteoric waters have been extensively used to identify the main sources of water evaporation (Merlivat & Jouzel 1979; Uemura *et al.* 2008), migration pathways of humid air masses (Masson-Delmotte *et al.* 2005; Vimeux *et al.* 2005; Guan *et al.* 2013), temperature effects under temperate climates (Dansgaard 1964; Yurtsever 1975; Rindsberger *et al.* 1983; Rozanski *et al.* 1993; Gat 1996), amount effects under humid tropical and equatorial areas (Dansgaard 1964; Rozanski *et al.* 1993), and the recycling of continental moisture released during the evaporation of soils, rivers, lakes and closed marine basins (Gat & Carmi 1970; Froehlich *et al.* 2008; Wang & Yakir 2000; Gibson & Edwards 2002; Aemisegger *et al.* 2014; Langman 2015; Wang *et al.* 2016; Juhlke *et al.* 2019).

$\delta^2\text{H}$ and $\delta^{18}\text{O}$ values of precipitations (rain, snow) follow an empirical linear relationship at the global scale that is called the Global Meteoric Water Line (GMWL: $\delta^2\text{H} = 8\delta^{18}\text{O} + 10$). It was defined for the first time by Craig (1961) and refined later by Dansgaard (1964) who considered mean isotopic compositions weighted by the amount of precipitation. Basically, the isotopic compositions obey a Rayleigh's distillation law in both evolving reservoirs of vapour water and condensed water. Moreover, condensation in clouds globally proceeds from warm low latitudes towards cold high latitudes. Air temperature in the residual cloud tends to decrease resulting in an increasing isotopic difference between precipitation and water vapour. The GMWL relationship is very useful in hydrology to correlate experimental data and to understand how the atmospheric water vapour forms the various sources of freshwater on the continents.

Craig (1961) observed that the GMWL does not pass through the $\delta^2\text{H}-\delta^{18}\text{O}$ composition of its source (SMOW), meaning that atmospheric vapour is not in equilibrium with seawater. Such pattern is mainly the consequence of the evaporation of the sea surface under an atmosphere with a relative humidity (RH) lower than 100%. Indeed, evaporation of water involves both equilibrium and kinetic effects whose respective magnitudes depend on temperature, relative humidity and wind velocity (Craig & Gordon 1965). Consequently, the slope and intercept values of the GMWL record the evaporative conditions (T, RH) that prevail at the source of the humid air masses.

However, it is of prime concern that large variations in the slope and intercept values are observed at the regional or local scale (Kendall & Coplen 2001; Sharp 2017). For example, the case of tropical islands with slopes close to 5 or 6 was identified in the pioneering study of Dansgaard (1964). Indeed, the geographic distribution of $\delta^{18}\text{O}$ and $\delta^2\text{H}$ values of precipitations also partly reflects the partition of climate modes at a regional scale. As underlined by Kendall and Coplen (2001), LMWL from the western and southern areas of USA have S lower than 6. Sharp (2007) concluded that the GMWL represents a weighted average of all LMWL which slopes are commonly lower than 8 with a large range of intercept values that may be either negative (down to -2) or positive (up to 15). Variations of slope and intercept values constitute a critical aspect when considering the objectives to reconstruct past climates on the basis of continental proxies. Consequently, the identification of regional processes needs to be integrated into models simulating past or future climates of the Earth, especially for glacial stages or super-greenhouse periods.

We have chosen the example of the European continent well documented by the isotopic data collected through time by the numerous IAEA sites. Europe is also characterized by one main source of precipitation that formed from the prevailing moisture-bearing westerly winds, except in the Mediterranean Basin. Indeed, the Mediterranean basin is characterized by a specific $\delta^{18}\text{O}-T$ relationship compared to the rest of Europe as shown, for example, by Gat & Carmi (1970) and Lécuyer *et al.* (2018). This area is characterized by specific patterns of atmospheric circulation with

dry and cold continental air masses that interact with a marine basin characterized by high evaporation rates and relative high sea surface temperatures ($\approx 20^\circ\text{C}$). Such air-sea interactions generate important sites of cyclogenesis, especially in the eastern part of the Mediterranean Sea.

Monthly weighted $\delta^2\text{H}$ and $\delta^{18}\text{O}$ values of precipitation have been therefore compiled from European IAEA stations, excluding areas that are under the regional climatic influence of the Mediterranean basin. Those data allowed the calculation of the slopes of the corresponding $\delta^2\text{H}-\delta^{18}\text{O}$ meteoric water lines determined for each station. The IAEA stations are widespread over a surface of about 10^7 km^2 . This study aims to demonstrate that changes in S values of the local meteoric water line track the evolution of a humid air mass that progressively condenses eastward over Europe. Increasing slopes S record the increasing degree of continentality that are defined here by indices quantifying the intra-annual temperature and precipitation amplitudes. We also show the important role of the dew point of a humid air mass that partly controls the slope S of meteoric water lines under mid latitudes. The influence of neighbouring water masses (oceans, close marine basins and lakes) on the amount of vapour water potentially recycled into local precipitations is also discussed.

Basic principles

Continentality

IAEA stations are geo-referenced in terms of latitude (λ) and longitude (ϕ) coordinates. Since the beginning of the XXth century, indices of continentality have been proposed. Conrad (1946)'s K index, derived from Gorczyński (1920) and Johansson (1926)'s ones, depends on A_T , the temperature difference between the warmest and the coldest month of the year, and is defined as follows:

$$K = \frac{1.7A_T}{\sin(\lambda+10)} - 14 \quad (1)$$

This continentality index K has been revised by Hela (1953) as follows:

$$K = \frac{1.97A_T}{0.92+\sin(\lambda-53)} - 13.3 \quad (2)$$

These equations are all based on two boundary conditions that are an index of 0 for a theoretical oceanic climate without any influence of emerged lands and an index of 100 for a continental climate without any influence of a water mass.

Relative Humidity and Dew Point

The relative humidity RH (in %) is basically the ratio between the actual water vapour pressure P_w and the saturation water vapour pressure (P_s):

$$RH = \frac{P_w}{P_s} 100 \quad (3)$$

with

$$P_s = C \cdot \exp \frac{(A \cdot T)}{(B+T)} \quad (4)$$

and

$$P_w = \frac{nRT}{V} \quad (5)$$

T and V are respectively the temperature and the volume of the gas mixture, R is the ideal gas constant and n is the number of moles of water vapour. $A = 7.625$, $B = 243.04^\circ\text{C}$ and $C = 610.94 \text{ Pa}$.

The Dew Point (T_d), expressed in $^\circ\text{C}$, is the temperature a humid air mass should have to start condensing water. In other words, T_d represents the temperature at which the actual water vapour pressure equals the saturated water vapour pressure ($RH = 100\%$). Several empirical equations have been derived these last decades from Magnus (1844)'s equation. Various set of fitting parameters are available in the literature. Here, we propose to refer to a review of these equations and parameters according to Gibbins (1990), Alduchov & Eskridge (1996) and Lawrence (2005). In practice, the dew point T_d is usually calculated from RH:

$$T_d = \frac{B \left[\ln \left(\frac{RH}{100} \right) + \frac{AT}{B+T} \right]}{A - \ln \left(\frac{RH}{100} \right) - \frac{AT}{B+T}} \quad (6)$$

where T is the air temperature (“dry-bulb temperature”) in °C. This equation applies for $RH > 0$ over the temperature range $-40^\circ\text{C} \leq T \leq +50^\circ\text{C}$. For a RH of 100, T_d equals T while at $RH < 100\%$ T_d is always lower than T. At the surface of the Earth, T_d varies from $+30^\circ\text{C}$ under equatorial and humid tropical belts down to -40°C at the poles and under high-latitude continental areas such as Canada and Siberia (Mourshed, 2016).

Slopes of Meteoric Water Lines (MWL) and deuterium-excess

Starting from a generic formulation of the linear equation describing the Global Meteoric Water Line (GMWL) expressed as follows:

$$\delta^2\text{H} = S \cdot \delta^{18}\text{O} + b \quad (7)$$

with ‘S’ being the slope and ‘b’ the intercept of the linear equation. For a slope $S = 8$, the intercept ‘b’ is called the “deuterium excess” (*d* or *d*-excess) defined for the first time by Dansgaard (1964).

Indeed, during evaporation of a water mass, the water vapour is less depleted in deuterium than in ^{18}O as a consequence of the differential rates of diffusivity of water isotopologues at the interface where the transition between the two states of water takes place. This parameter is especially sensitive to the physical conditions (temperature and moisture content of the air) prevailing during the evaporation of the sea surface (Merlivat & Jouzel 1979; Johnsen *et al.* 1989; Pfahl & Wernli 2008). Craig (1961) found that the global mean meteoric water has a *d*-excess of 10‰, reflecting sea surface waters out of equilibrium with the atmosphere. This deuterium excess corresponds to a temperature close to 25°C and a mean relative humidity lower than 100% at the seawater-atmosphere interface. More precisely, Merlivat and Jouzel (1979) computed a RH value of 81% and a temperature of evaporation of 26°C for the GMWL equation determined by Craig (1961) while comparable values were obtained for Dansgaard (1964) equation (RH = 79.5% and $T = 25.4^\circ\text{C}$). It is worthy to note here that a higher value of 85% for RH was proposed by Clark and Fritz (1997). Slope S is an interesting second-order

parameter as its relative variation can be analysed independently of a reference linear equation such as the GMWL ($S = 8$; $d = 10$):

$$S = (\delta^2\text{H} - b)/\delta^{18}\text{O} \quad (8)$$

This slope S corresponds to the ratio between the isotopic fractionation factors α defined for the two isotopic systems at equilibrium between the two co-existing water phases, which means liquid water and water vapour or water ice and water vapour. In the case of the liquid water \rightleftharpoons water vapour state change, the mean slope S is expressed as follows:

$$S = \frac{\left(\frac{{}^2\text{H}}{{}^1\text{H}}\right)_{\text{liquid}} - 1}{\left(\frac{{}^2\text{H}}{{}^1\text{H}}\right)_{\text{vapour}} - 1} = \frac{\alpha^2_{(\text{liquid-vapour})} - 1}{\alpha^{18}_{(\text{liquid-vapour})} - 1} \quad (9)$$

$$\frac{\left(\frac{{}^{18}\text{O}}{{}^{16}\text{O}}\right)_{\text{liquid}} - 1}{\left(\frac{{}^{18}\text{O}}{{}^{16}\text{O}}\right)_{\text{vapour}} - 1}$$

The rainfall is usually considered at isotopic equilibrium with vapour because the formation of water droplets in clouds takes place when saturation or oversaturation in water vapour is reached.

Monthly $\delta^2\text{H}$ and $\delta^{18}\text{O}$ values of precipitation have been compiled from European IAEA stations

(Figure 1A) along with the linear relationship for Europe illustrated in Supplementary Figure 1. Local Meteoric Water Lines (LMWL) were generated using weighted averages of monthly precipitation over several years. The slopes S of the $\delta^2\text{H}$ - $\delta^{18}\text{O}$ LMWL, determined for each station, are considered hereafter.

Filtering of data

Several criteria were used to filter the database as follows:

- Stations that are under the regional climatic influence of the Mediterranean basin were excluded. Indeed, The Mediterranean basin is characterized by a specific $\delta^{18}\text{O}-\text{T}$ relationship compared to the rest of Europe as shown, for example, by Gat & Carmi (1970) and Lécuyer *et al.* (2018). This area is characterized by specific patterns of atmospheric circulation with dry and cold continental air masses that interact with a marine basin characterized by high evaporation rates and relative high sea surface temperatures ($\approx 20^\circ\text{C}$). Such air-sea interactions favor the genesis of cyclones, especially in the eastern part of the Mediterranean Sea. The Mediterranean climate is characterized by warm to hot dry summers along with mild and wet winters (see Lionello *et al.* 2006 for a detailed definition). It corresponds to a geographic area located on the west side of continents between 30° and 40° of latitude in the vicinity of a large mass of water (Figure 1B).

- Stations located at elevations equal to or higher than 1000 m were discarded to avoid isotopic effects related to the orographic lifting of humid air masses.

- LMWL have only been calculated for stations for which at least 5 years of record are available with at least 9 months recorded in the year in order to increase the robustness of the database.

- Only LMWL characterized by robust coefficients of determination ($R^2 \geq 0.75$) have been kept in the final database. Most IAEA stations have $R^2 \geq 0.9$ and the median value is 0.98 (Supplementary Figure 2).

Finally, filtered data allowed the calculation of the slopes of the corresponding $\delta^2\text{H}-\delta^{18}\text{O}$ LMWM determined for each station (see Supplementary Table 1). One example is provided with the IAEA station in Berlin, Germany (Figure 2). Slopes S of LMWL have been ultimately correlated to the longitude of IAEA stations, the annual amplitude of air temperatures and precipitation, the Hela index K of continentality and the mean annual dew point.

Results

Continentality

Studied European IAEA stations range from -10°W to 57°E in longitude and from 42°N to 69°N (Figure 1A). The index K of continentality (Hela 1953) increases significantly eastward (Figure 3A) according to equation (10):

$$K = 0.62(\pm 0.05)\phi + 32.47(\pm 1.00) \text{ with } R^2 = 0.70 \quad (10)$$

Amplitudes in temperature T_A increase with ϕ (Figure 3B) according to equation (11):

$$T_A = 0.37(\pm 0.01)\phi + 14.23(\pm 0.28) \text{ with } R^2 = 0.91 \quad (11)$$

It is worthy to note that the temperature amplitude in our data set is strongly correlated with the longitude but not the latitude. This last observation is not consistent with the well-known increase in temperature amplitude with increasing latitude at the global scale, as mentioned by Hela (1953). The apparent paradox between our observations and this basic principle is mostly solved by considering the Southwest – Northeast distribution of the IAEA stations, which results in a positive relation between latitude and longitude (Figure 1A). We can also consider that the northwestern part of Europe receives a sizable amount of heat from the Gulf Stream, which contributes to reduce the latitudinal temperature gradient. Consequently, most IAEA stations have longitudes that increase with latitudes (Figure 3C).

Relative Humidity and Dew Point

According to maps computed by Mourshed (2016), the mean annual Dew Point values decrease over Europe along a southwest–northeast gradient, from about 15°C in Portugal down to about -20°C in Russia. Along this gradient, the mean air temperature (MAT) ranges from $+17^{\circ}\text{C}$ to -1°C and RH values increase from about 35% up to 75% in July and from about 50-55% to 85-90% in January (NCARS 2017; Wypych *et al.* 2018). Seasonal variations in T_d values (negative in winter, positive in

summer) are highly contrasted for IAEA stations located far inland (see for example Berlin, Germany and Arkhangelsk, Russia) while they are rather limited (a few degrees in the positive values) for western coastal locations such as La Coruna, Spain, or islands such as Valentia, Ireland.

The slope S

Slope S of LMWL recorded at European IAEA stations are reported versus ϕ (Figure 4A). These slopes range from about 6 to 10, although three stations (Odessa, Ukraine; Riga, Latvia and St. Petersburg, Russia) display quite large standard deviations around the mean, two of them, with the highest slope values close to 10, being outliers (Riga and St. Petersburg). In this data set, S regularly increases eastward (Figure 4B) and is best described by a logarithmic fitting as follows:

$$S = 2.45(\pm 0.25)\log_{10}(\phi+15) + 4.13\pm(0.35) \text{ with } R^2 = 0.60 \quad (12)$$

The value of 15 added to ϕ was arbitrary chosen to make all the longitude values positive.

Interpretation of data and discussion

Slope of the LWML as a function of equilibrium temperature

Genesis of rain or snow during the condensation of cloud water vapour is considered as an isotopic equilibrium process, hence only related to air temperature (Juhlke *et al.* 2019). According to this model, the hydrogen and oxygen isotope ratios of precipitation are highly sensitive to the latitude and altitude of the site as well as air temperature (Rozanski *et al.* 1993). The stable isotope compositions also correlate with increasing continentality because of the successive precipitation events that obey the Rayleigh distillation process (Clark & Fritz 1997; Gat *et al.* 2001).

Several temperature-dependent isotope fractionation equations have been published so far in the scientific literature for both $^2\text{H}/^1\text{H}$ and $^{18}\text{O}/^{16}\text{O}$ fractionations between liquid water and vapour water (Halas 2008). A pioneering experimental study was performed by Majoube (1971) who proposed the two following isotopic fractionation equations determined in the temperature range 0°C – 100°C :

$$\ln^{18} \alpha_{(\text{liq-vap})} = 1.137(10^3 \cdot T^{-2}) - 0.4156(T^{-1}) - 2.066 \times 10^{-3} \quad (13)$$

$$\ln^2 \alpha_{(\text{liq-vap})} = 28.844(10^3 \cdot T^{-2}) - 76.248(T^{-1}) + 52.612 \times 10^{-3} \quad (14)$$

Comparable equations have also been experimentally determined by Horita & Wesolowski (1994) in the temperature range 25°C–350°C:

$$10^3 \ln^{18} \alpha_{(\text{liq-vap})} = -7.865 + 6.7123(10^3 \cdot T^{-1}) - 1.6664(10^6 \cdot T^{-2}) + 0.35041(10^9 \cdot T^{-3}) \quad (15)$$

$$10^3 \ln^2 \alpha_{(\text{liq-vap})} = 1158.8(T^3 \cdot 10^{-9}) - 1620.1(T^2 \cdot 10^{-6}) + 794.84(T \cdot 10^{-3}) - 161.04 + 2.9992(10^9 \cdot T^{-3}) \quad (16)$$

Of great importance for the understanding of the isotopic composition of precipitation, which takes place in the atmosphere below the “freezing level” or 0°C isotherm, is the knowledge of the isotopic fractionations between water ice and water vapour. For example, Majoube (1970) proposed the following equation for the oxygen isotopes in the temperature range -30°C to 0°C:

$$10^3 \ln^{18} \alpha_{(\text{ice-vap})} = -28.224 + 11.839(10^3 \cdot T^{-1}) \quad (17)$$

while Merlivat & Nief (1967) proposed the following equation for the $^2\text{H}/^1\text{H}$ system in the temperature range -30°C to 0°C:

$$10^3 \ln^2 \alpha_{(\text{ice-vap})} = -94.5 + 16.289(10^6 \cdot T^{-2}) \quad (18)$$

Using equations (15) to (18), we define $S = (\alpha^2\text{H}-1)/(\alpha^{18}\text{O}-1)$ for the liquid water–water vapour and water ice–water vapour systems as functions of temperature (Figure 5). We also emphasize that T_d values over Europe are compatible with S increasing eastward from ≈ 6 to ≈ 9). Supercooled water droplets may form in high-altitude clouds at temperatures as low as -40°C . In this case, S would approach a value close to 9 (Figure 4B).

Sources of air moisture over Europe

Moisture over Europe is mainly transported by the westerlies that carry the vapour generated by the evaporation of the Central and North Atlantic surface waters. Outside the area under the Mediterranean influence, moisture over Europe mainly comes from the Central and North Atlantic surface waters, and is transported eastwards by the westerlies. Arctic winds, bringing moisture from the Norwegian Sea, can reach Europe during winter.

Westerlies bring to western Europe warm and humid air masses responsible for large amounts of precipitation during winter and the intermediate seasons. During summer, westerlies tend to bring cooler air than that present over the continent (Barriopedro *et al.* 2014). At a synoptic scale and assuming a closed water cycle (e.g. Jouzel *et al.* 1997), deuterium excess content of average oceanic water vapour at the site of evaporation is mainly controlled by relative humidity (RH), sea surface temperature (SST) and, to a lesser extent, wind velocity, (Merlivat & Jouzel 1979; Aemisegger *et al.* 2014). Precipitation along the GMWL is generated from a vapour formed at RH and SST values of 85% and 25°C , respectively (Clark & Fritz 1997). Several linear relationships between RH and SST have been established yet (Merlivat & Jouzel 1979; Jouzel *et al.* 1996; Pfahl & Wernli 2008; Aemisegger *et al.* 2014; Pfahl and Sodemann, 2014). All of them indicate that the deuterium excess increases with temperature and decreases with RH ($d = 0$ for $\text{RH} = 100\%$). In other words, it means that for temperatures higher than 25°C and RH lower than 85% at the source of evaporation, the first generated LMWL will have a slope lower than 8. Indeed, LMWL

with low slopes, as low as 5, have been observed and discussed by Dansgaard (1964) in the case of several tropical islands such as Hawaii, USA. Dansgaard (1964) considered that such low slopes close to 5 cannot be explained by a “*simple Rayleigh condensation process under equilibrium conditions ... since the calculation on such processes gives 7.5*”. Indeed, a cloud can receive additional vapour from local oceanic sources along its travel path and this vapour might not be strictly produced under equilibrium conditions but to some extent by kinetic/non-equilibrium isotopic fractionation because of the fast evaporation process. In the case of the Atlantic Ocean and the western European coast, we can suspect that humid air masses are fed by moisture derived from a nearby evaporating oceanic surface. Such process may explain why LMWL recorded at stations located along the western Atlantic coast (La Coruna, Spain; Valentia, Ireland; Wallingford and Keyworth, UK) have slopes close to 6 instead of 8.

Slopes of MWL over Europe tend to slightly increase eastward even if we do not take into account the large potential reservoir of moisture represented by the Atlantic Ocean bathing the western coast of Europe (called here “Atlantic Side Effect”). It is worthy to note that the origin of precipitation at a regional scale can generally be ascribed to three main sources that are local soil evaporation, plant transpiration and externally advected moisture (Bisselink & Dolman 2008).

According to Gibson & Edwards (2002), soil-derived moisture is depleted in ^{18}O and ^2H relative to its source while transpiration does not produce isotopic fractionation between moisture and soil water because “*the transfer of moisture to the atmosphere by plants is essentially quantitative, and heavy-isotope enrichment is restricted to internal plant waters*”.

About 60% of the total evapotranspiration flux over land enters the atmosphere via transpiration (Schlesinger & Jasechko 2014), which means that local soil evaporation represents about 40% of the total flux of recycled moisture (Trenberth 1999; Bisselink & Dolman 2008; Froehlich *et al.* 2008; Kong *et al.* 2013; Wang *et al.* 2016; Wypych *et al.* 2018). In Europe, the atmospheric water vapour

content, which depends on air temperature, decreases along a southwest-northeast gradient except during the summer season (Wypych *et al.* 2018). Indeed, water vapour pressure decreases from about 15 to 5 kg.m⁻² in January, and from about 20 to 10 kg.m⁻² in April and October, and increases from about 20 to 30 kg.m⁻² in July (Wypych *et al.* 2018). Recycling of soil moisture mixed with the externally advected moisture carried out by the westerlies may contribute to decrease the slope of LMWL at the westernmost stations.

Rain drops are subject to evaporation during their fall, in particular when they travel through a dry and warm column of air (Stewart 1975). Evaporation of rain drops is known to change dramatically the original composition of rainfall in the warmest and driest regions of the world such as Central-Eastern Africa (Balagizi *et al.* 2018; Balagizi & Liotta 2019). Under unsaturated conditions, i.e. RH < 100%, differences in diffusivity coefficients between H₂O isotopologues (Merlivat 1978; Luz *et al.* 2009) induce out of equilibrium isotopic fractionations. As a result, the ratio between ²H/¹H and ¹⁸O/¹⁶O in the rainfall reaching the ground differs from the one in the cloud vapour. Albeit to a lesser degree, evaporation of falling water drops may decrease the slope of the LMWL in southwest Europe, which is characterized by low RH in January (RH ≈ 50%) and July (RH ≈ 40%) according to data provided by Wypych *et al.* (2018). In addition, mild to warm temperatures prevail all year round with daily temperatures that can exceed 30°C during summer.

Finally, in the case of Europe, it is expected from the reasoning mentioned above that the slope S of the $\delta^2\text{H}-\delta^{18}\text{O}$ line would increase as the clouds are progressively moving away from the Atlantic side. Equations that describe ²H/¹H and ¹⁸O/¹⁶O fractionations at thermodynamic equilibrium during phase changes (liquid water ⇌ water vapour and water ice ⇌ water vapour) predict slopes in the range 8.5–10 as it observed in the easternmost part of Europe.

Implications for paleoclimatic reconstructions

Present-day GMWL and LMWL are most likely valid for the Holocene but risky to apply to older periods, especially glacial stages for which RH and prevailing winds may differ from today and have strong impacts at least on the intercept of linear equations (Merlivat and Jouzel, 1979). Moreover, changes in continental ice volume have direct consequences on the $\delta^{18}\text{O}$ of the global ocean (Lambeck et al., 2014) from which precipitations ultimately derive. The variations in slopes and intercepts of LMWL we observed over Europe also mean that the relationships between air temperature and $\delta^{18}\text{O}$ of precipitation vary from one location to another. At a regional scale, robust linear relationships have been evidenced between mean air temperature (MAT) and oxygen isotope compositions of precipitation ($\delta^{18}\text{O}_{\text{mw}}$) for Europe (Mediterranean Basin excluded; Lécuyer 2013):

$$\text{MAT } (^{\circ}\text{C}) = 1.41(\pm 0.09) \delta^{18}\text{O}_{\text{mw}} + 22.02(\pm 0.83) \text{R}^2 = 0.79 \quad (19)$$

At a local scale in the studied Europe area, we also observe some differences in mean annual and seasonal patterns of air temperatures between La Coruna, Valentia, Wallington, Berlin, Kalinin and Arkhangelsk (Figure 1A), which are IAEA stations selected for the demonstration, and located along a southwest-to-northeast gradient. La Coruna, Spain and Valentia, Ireland, are two cities located along the westernmost side of the Atlantic coast (Figure 1A). They are both characterized by low slope values of their LMWL, positive correlations between $\delta^{18}\text{O}_{\text{mw}}$ and monthly mean air temperatures, while strong negative correlations are observed between $\delta^{18}\text{O}_{\text{mw}}$ and monthly mean precipitations (Supplementary Table 2). Both locations share relative dry summers and rainy winters. Using equation (19) as a reference for Europe would allow mean air temperatures to be overestimated by a few degrees (between 3°C and 4°C) for Valentia, Ireland, while air temperatures calculated at La Coruna, Spain, would match that deduced from the local equation (Supplementary Table 2). Wallingford, UK, is located in south England inland, the slope of its LMWL is higher ($S \approx 6.6$) than for the two previous mentioned IAEA stations, $\delta^{18}\text{O}_{\text{mw}}$ are strongly and positively correlated with air temperatures while they are poorly and negatively correlated with precipitations (Supplementary

Table 2). Error in the estimate of air temperature using equation (19) would be only 1°C by reference to the local equation. Finally, eastward, Berlin, Germany, Kalinin and Arkhangelsk, Russia, are characterized by “continental-boreal” climatic conditions (Figure 1B) and they have the highest S of 7.97, 8.43 and 8.53 for their LMWL, respectively. $\delta^{18}\text{O}_{\text{mw}}$ display strong and positive correlations with air temperatures and weaker but positive correlations with precipitations (Supplementary Table 2). Those three locations share relative wet summers and less humid winters. Estimates of air temperatures using equation (19) do not allow errors larger than 1°C by reference to local equations (Supplementary Table 2).

Reconstructions of air temperatures in Europe during the Holocene have been commonly performed on the basis of global or regional equations relating $\delta^{18}\text{O}_{\text{mw}}$ to air temperatures that were applied to the $\delta^{18}\text{O}$ of lacustrine carbonates (Hammarlund *et al.* 2002; Makhnach *et al.* 2004), speleothems (Denniston *et al.* 1999; Lechleitner *et al.* 2018 and references therein), invertebrate remains such as aragonite from mollusc shells (Baroni *et al.* 2006; Leng & Lewis 2016) and vertebrate remains of mammal teeth (Iacumin *et al.* 2004; Pilaar Birch *et al.* 2016). Fossil remains of invertebrates or vertebrates are generally retrieved from specific locations and their oxygen isotope compositions mostly record local climatic conditions. Moreover, some fossil remains such as rodent teeth (Royer *et al.* 2013) or earthworm calcite granules (Prud’homme *et al.* 2016) are known to only record the warmest months of the year. In areas characterized by a strong air temperature seasonality (e.g. Germany, Russia), errors in the calculation of air temperatures, which are based on the $\delta^{18}\text{O}$ of either apatite phosphate or calcite, may exceed 5°C when using equation (19) (Supplementary Table 2).

Our study shows that it is tricky to apply regional or global-scale relationships between air temperature and $\delta^{18}\text{O}_{\text{mw}}$ to local isotopic records. Error estimates in air temperatures reconstructions may reach several degrees, either underestimating or overestimating real temperatures that prevailed during the life of animals. Therefore, we emphasize that distinct and appropriate equations must be applied, for example, to the Iberian Peninsula, for which a large surface is under the influence of the

Mediterranean climate while the remaining one is exposed to the Atlantic seaside. As a general rule, equations differ between the southwest-west part of Europe with warm temperate and “oceanic” climate conditions and the north-northeast one that is characterized by cold temperate and continental or boreal climate conditions.

Improved modelling of the past water cycle with an increased spatial resolution should provide the appropriate LMWL equations and those relating T to $\delta^{18}\text{O}_{\text{mw}}$. It is of paramount importance if we want to bear in mind the objectives of connecting faunal assemblages, migration pathways, and the presence of human beings to climate dynamics during the Holocene.

Conclusions

Monthly weighted $\delta^2\text{H}$ and $\delta^{18}\text{O}$ values of precipitation have been compiled from European IAEA stations, excluding areas that are under the regional climatic influence of the Mediterranean basin. Those data allowed the calculation of the slopes S of the corresponding $\delta^2\text{H}$ – $\delta^{18}\text{O}$ local meteoric water lines (LMWL) determined for each station. For linear relationships defined over periods of at least five years and characterized by a coefficient of determination higher than 0.75, S increases with longitude ϕ from ≈ 5 (Portugal) to ≈ 9 (Russia). S are positively correlated to relative air humidity, and continentality, which is quantified by the intra-annual amplitude of air temperatures. On the basis of our knowledge of isotopic fractionation that takes place during water phase changes, S close to 9 are expected to reflect hydrogen and oxygen isotope fractionation close to equilibrium during condensation of water vapour into liquid water or snow. Slopes that tend to decrease down to 5 are interpreted, in most cases, as the result of an increasing recycling of water vapour derived from the surface of the nearby oceanic waters (“Atlantic Side Effect”). In addition to this process, enrichment in heavy isotopes also took place in southwest Europe during the partial evaporation of water droplets during their fall in air of relative low humidity and cool to warm temperature.

Variations in slopes and intercepts of LMWL at a local scale over Europe also imply distinct linear equations between air temperature T and $\delta^{18}\text{O}$ of precipitation. Consequently, shifts in air temperature

estimates relative to an equation established at a regional scale ($\approx 10^7 \text{ km}^2$) may reach a few °C. Such isotopic properties of the water cycle put severe limitations on the use of regionally-based $T-\delta^{18}\text{O}_{\text{mw}}$ equations applied to the oxygen isotope compositions of biogenic calcium carbonates and phosphates that constitute the skeletons of most invertebrates and vertebrates. Distinct and appropriate equations must be established for sub-regions such as the Iberian Peninsula, the southwest and west Atlantic seaside and the east-northeast European areas.

The authors are grateful to Prof. Kazimierz Rozanski for preliminary discussions and his advice that contributed to improve the scientific content of this study. Ph. Boulvais and one anonymous reviewer are also thanked for their helpful and constructive comments and suggestions that helped us to improve the scientific content of this study.

ACCEPTED MANUSCRIPT

References

- Aemisegger, F., Pfahl, S., Sodemann, H., Lehner, I., Seneviratne, S.I. and Wernli, H. 2014. Deuterium excess as a proxy for continental moisture recycling and plant transpiration. *Atmospheric Chemistry and Physics*, **14**, 4029–4054.
- Alduchov, O.A. and Eskridge, R.E. 1996. Improved Magnus form approximation of saturation vapor pressure. *Journal of Applied Meteorology*, **35**, 601–609.
- Angert, A., Lee, J.-E. and Yakir, D. 2008. Seasonal variations in the isotopic composition of near-surface water vapour in the eastern Mediterranean. *Tellus*, **60B**, 674–684.
- Balagizi, C.M. and Liotta, M. 2019. Key factors of precipitation stable isotope fractionation in Central-Eastern Africa and Central Mediterranean. *Geosciences*, **9**, 337. DOI: 103390/geosciences9080337
- Balagizi, M.C., Kasereka, M.M., Cuoco, E. and Liotta, M. 2018. Influence of moisture source dynamics and weather patterns on stable isotopes ratios of precipitation in Central-Eastern Africa. *Sciences of the Total Environment*, **628**, 1058–1078.
- Baroni, C., Zanchetta, G., Fallick, A.E. and Longinelli, A. 2006. Mollusca stable isotope record of a core from Lake Frassino, northern Italy: hydrological and climatic changes during the last 14 ka. *The Holocene*, **16**, 827–837.
- Barriopedro, D., Gallego, D., Alvarez-Castro, M.C., García-Herrera, R., Wheeler, D., Peña-Ortiz, C. and Barbosa, S.M. 2014. Witnessing North Atlantic westerlies variability from ships' logbooks (1685–2008). *Climate dynamics*, **43**, 939–955.
- Bisselink, B. and Dolman, A.J. 2008. Precipitation recycling: Moisture sources over Europe using ERA-40 data. *Journal of Hydrometeorology*, **9**, 1073–1083.
- Clark, I.D. and Fritz, P. 1997. The environmental isotopes. *Environmental Isotopes in Hydrogeology*, pp. 312.
- Conrad, V. 1946. Usual formulas of continentality and their limits of validity. *Transactions of the American Geophysical Union*, **27**, 663–664.
- Craig, H. 1961. Isotopic variations in meteoric waters. *Science*, **133**, 1702–1703.

- Craig, H. and Gordon, L.I. 1965. Deuterium and oxygen-18 variations in the ocean and the marine atmosphere. In *Stable Isotopes in Oceanographic Studies and Paleotemperatures* (ed. E. Tongiorgi.). Lab. Geol. Nucl. pp. 9-130.
- Dansgaard, W. 1964. Stable isotopes in precipitation. *Tellus*, **16**, 436–468.
- Denniston, R.F., Gonzalez, L.A., Semken, H.A., Asmerom, Y., Baker, R.G., Recelli-Snyder, H., Reagan, M.K. and Bettis III, E.A. 1999. Integrating stalagmite, vertebrate, and pollen sequences to investigate Holocene vegetation and climate change in the southern Midwestern United States. *Quaternary Research*, **52**, 381-387.
- Froehlich, K., Kralik, M., Papesch, W., Rank, D., Scheifinger, H. and Stichler, W. 2008. Deuterium excess in precipitation of Alpine regions—moisture recycling. *Isotopes in Environmental and Health Studies*, **44**, 61-70.
- Gat, J.R. and Carmi, H. 1970. Evolution of the isotopic composition of atmospheric waters in the Mediterranean Sea area. *Journal of Geophysical Research*, **75**, 3039–3040.
- Gat, J.R. 1996. Oxygen and hydrogen isotopes in the hydrologic cycle. *Annual Review of Earth and Planetary Sciences*, **24**, 225–262.
- Gat, J.R., Mook, W.G. and Meijer, H.A. 2001. Environmental isotopes in the hydrological cycle. Principles and Applications. *UNESCO/IAEA Series*, **2**, pp. 114.
- Gibbins, C.J. 1990. A survey and comparison of relationships for the determination of the saturation vapour pressure over plane surfaces of pure water and of pure ice. *Annales Geophysicae*, **8**, 859–885.
- Gibson, J.J. and Edwards, T.W.D. 2002. Regional water balance trends and evaporation-transpiration partitioning from a stable isotope survey of lakes in northern Canada. *Global Biogeochemical Cycles*, **16**, 1026. DOI: 10.1029/2001GB001839.
- Gorczyński, L. 1920. Sur le calcul du degré du continentalisme et son application dans la climatologie. *Geografiska Annaler*, **2**, 324–31.
- Guan, H., Zhang, X., Skrzypek, G., Sun, Z. and Xu, X. 2013. Deuterium excess variations of rainfall events in a coastal area of South Australia and its relationship with synoptic weather systems and atmospheric moisture sources. *Journal of Geophysical Research: Atmospheres*, **118**, 1123–1138.

- Halas, S., 2008. About isotope equilibrium between liquid and vapour phases. *Isotopes in Environmental and Health Studies*, **44**, 129–135.
- Hammarlund, D., Barnekow, L., Birks, H.J.B., Buchardt, B. and Edwards, T.W. 2002. Holocene changes in atmospheric circulation recorded in the oxygen-isotope stratigraphy of lacustrine carbonates from northern Sweden. *The Holocene*, **12**, 339–351.
- Hela, I. 1953. Regional distribution of the continentality in the climate of the oceans. *Geophysica (Helsingfors)*, **4**, 41–47.
- Horita J. and Wesolowski D.J. 1994. Liquid-vapor fractionation of oxygen and hydrogen isotopes of water from the freezing to the critical temperature. *Geochimica et Cosmochimica Acta*, **58**, 3425–3437.
- Iacumin, P., Nikolaev, V., Genoni, L., Ramigni, M., Ryskov, Y. G. and Longinelli, A. 2004. Stable isotope analyses of mammal skeletal remains of Holocene age from European Russia: a way to trace dietary and environmental changes. *Geobios*, **37**, 37–47.
- Johansson, O. V. (1926). Über die Asymmetrie der meteorologischen Schwankungen. *Societas Scientiarum Fennica. Commentationes Physico-Mathematicae*, **3**, 1, Helsingfors.
- Johnsen, S.J., Dansgaard, W. and White, J.W.C. 1989. The origin of Arctic precipitation under present and glacial conditions. *Tellus B: Chemical and Physical Meteorology*, **41**, 452–468.
- Jouzel, J., Froehlich, K. and Schotterer, U. 1997. Deuterium and oxygen-18 in present-day precipitation: data and modelling. *Hydrological Sciences Journal*, **42**, 747–763.
- Jouzel, J., Koster, R.D., Suozzo, R.J. and Russell, G.L. 1994. Stable water isotope behavior during the last glacial maximum: A general circulation model analysis. *Journal of Geophysical Research: Atmospheres*, **99**, 25791–25801.
- Juhlke, T.R., Meier, C., van Geldern, R., Vanselow, K.A., Wernicke, J., Baidulloeva, J., Barth, J.A.C. and Weise, S.M. 2019. Assessing moisture sources of precipitation in the Western Pamir Mountains (Tajikistan, Central Asia) using deuterium excess. *Tellus B: Chemical and Physical Meteorology*, **71**, 1–16.
- Kendall, C. and Coplen, T.B. 2001. Distribution of oxygen-18 and deuterium in river waters across the United States. *Hydrological processes*, **15**, 1363–1393.

- Kong, Y., Pang, Z. and Froehlich, K. 2013. Quantifying recycled moisture fraction in precipitation of an arid region using deuterium excess. *Tellus B: Chemical and Physical Meteorology*, **65**, 19251. DOI: 10.3402/tellusb.v65i0.19251.
- Lambeck, K., Rouby, H., Purcell, A., Sun, Y., Sambridge, M. 2014. Sea level and global ice volumes from the Last Glacial Maximum to the Holocene. *Proceedings of the National Academy of Sciences*, **111**, 15296–15303.
- Langman, J.B. 2015. Spatial distribution of $\delta^2\text{H}$ and $\delta^{18}\text{O}$ values in the hydrologic cycle of the Nile Basin. *Journal of Arid Land*, **7**, 133–145.
- Lawrence, M.G. 2005. The relationship between relative humidity and the dewpoint temperature in moist air: A simple conversion and applications. *Bulletin of the American Meteorological Society*, **86**, 225–234.
- Lechleitner, F.A., Amirnezhad-Mozhdehi, S., Columbu, A., Comas-Bru, L., Labuhn, I., Pérez-Mejías, C. and Rehfeld, K. 2018. The potential of speleothems from Western Europe as recorders of regional climate: a critical assessment of the SISAL database. *Quaternary*, **1**, 30. doi:10.3390/quat1030030.
- Lécuyer, C. 2013. *Water on Earth*. John Wiley & Sons, 260 pp.
- Lécuyer, C., Atrops, F., Amiot, R., Angst, D., Daux, V., Flandrois, J.P., Fourel, F., Rey, K., Royer, A., Seris, M., Touzeau, A. and Rousseau, D.-D. 2018. Tsunami sedimentary deposits of Crete records climate during the ‘Minoan Warming Period’ (≈ 350 yr BP). *The Holocene*, **28**, 914–929.
- Leng, M.J. and Lewis, J.P. 2016. Oxygen isotopes in Molluscan shell: applications in environmental archaeology. *Environmental Archaeology*, **21**, 295–306.
- Lionello, P., Malanotte-Rizzoli, P., Boscolo, R., Alpert, P., Artale, V., Li, L., Luterbacher J., May, W., Trigo, R., Tsimplis, M., Ulbrich, U. and Xoplaki, E. (2006). The Mediterranean climate: An overview of the main characteristics and issues. *Developments in Earth and Environmental Sciences*, **4**, 1–26.
- Luz B., Barkan E., Yam R. and Shemesh A. (2009) Fractionation of oxygen and hydrogen isotopes in evaporating waters. *Geochimica et Cosmochimica Acta*, **73**, 6697–6703.
- Magnus, G., 1844. Versuche ubder die Spannkrafte des Wasserdampfes. *Annalen der Physik und Chemie*, **137**, 225–247.

- Majoube, M. 1970. Fractionation factor of ^{18}O between water vapour and ice. *Nature*, **226**, 1242–1242.
- Majoube, M. 1971. Fractionnement en oxygene-18 et en deuterium entre l'eau et sa vapeur. *Journal de Chimie Physique*, **68**, 1423–1436.
- Makhnach, N., Zernitskaja, V., Kolosov, I. and Simakova, G. 2004. Stable oxygen and carbon isotopes in Late Glacial–Holocene freshwater carbonates from Belarus and their palaeoclimatic implications. *Palaeogeography, Palaeoclimatology, Palaeoecology*, **209**, 73–101.
- Masson-Delmotte, V., Jouzel, J., Landais, A., Stievenard, M., Johnsen, S.J., White, J.W.C., Werner, M., Sveinbjornsdottir, A.E. and Fuhrer, K. 2005. GRIP deuterium excess reveals rapid and orbital-scale changes in Greenland moisture origin. *Science*, **309**, 118–121.
- Matthews, A., Ayalon, A. and Bar-Matthews, M. 2000. D/H ratios of fluid inclusions of Soreq cave (Israel) speleothems as a guide to the Eastern Mediterranean Meteoric Line relationships in the last 120 ky. *Chemical Geology*, **166**, 183–191.
- Merlivat, L., 1978. Molecular diffusivities of H_2^{16}O , HD^{16}O and HD^{18}O in gases. *Journal of Chemical Physics*, **69**, 2864–2871.
- Merlivat, L. and Jouzel, J. 1979. Global climatic interpretation of the deuterium–oxygen 18 relationship for precipitation. *Journal of Geophysical Research*, **84**, 5029–5033.
- Merlivat L. and Nief, G. 1967. Fractionnement isotopique lors des changements d'état solide-vapeur et liquide-vapeur de l'eau à des températures inférieures à 0°C . *Tellus*, **19**, 122–127.
- Mourshed, M. 2016. Climatic parameters for building energy applications: A temporal-geospatial assessment of temperature indicators. *Renewable energy*, **94**, 55–71.
- National Center for Atmospheric Research Staff 2017. The Climate Data Guide: Climate Forecast System Reanalysis. <https://climatedataguide.ucar.edu/climate-data/climate-forecast-system-reanalysis-cfsr>.
- Pfahl, S. and Sodemann, H. 2014. What controls deuterium excess in global precipitation? *Climate of the Past*, **10**, 771–781.
- Pfahl, S. and Wernli, H. 2008. Air parcel trajectory analysis of stable isotopes in water vapor in the eastern Mediterranean. *Journal of Geophysical Research*, **113**, D20104, doi:10.1029/2008JD009839.

- Pilaar Birch, S.E., Miracle, P.T., Stevens, R.E. and O'Connell, T.C. 2016. Late Pleistocene/Early Holocene Migratory Behavior of Ungulates Using Isotopic Analysis of Tooth Enamel and Its Effects on Forager Mobility. *PLoS ONE*, **11**, e0155714. Doi:[10.1371/journal.pone.0155714](https://doi.org/10.1371/journal.pone.0155714)
- Prud'homme, C., Lécuyer, C., Antoine, P., Moine, O., Hatté, C., Fourel, F., Martineau F. and Rousseau, D.-D. 2016. Palaeotemperature reconstruction during the Last Glacial from $\delta^{18}\text{O}$ of earthworm calcite granules from Nussloch loess sequence, Germany. *Earth and Planetary Science Letters*, **442**, 13–20.
- Rindsberger, M., Magaritz, M., Carmi, I. and Gilad, D. 1983. The relation between air mass trajectories and the water isotope composition of rain in the Mediterranean Sea area. *Geophysical Research Letters*, **10**, 43–46.
- Rozanski, K. 2005. Isotopes in Atmospheric Moisture. In: Aggarwal P.K., Gat J.R., Froehlich K.F. (eds) *Isotopes in the Water Cycle*. Springer, Dordrecht, pp. 291–302.
- Rozanski, K., Araguás-Araguás, L. and Gonfiantini, R. 1993. Isotopic patterns in modern global precipitation. *Washington DC American Geophysical Union Geophysical Monograph Series*, **78**, 1–36.
- Royer, A., Lécuyer, C., Montuire, S., Amiot, R., Legendre, S., Cuenca-Bescós, G., Jeannet, M. and Martineau, F. 2013. What does the oxygen isotope composition of rodent teeth record? *Earth and Planetary Science Letters*, **361**, 258–271.
- Schlesinger, W.H. and Jasechko, S. 2014. Transpiration in the global water cycle. *Agricultural and Forest Meteorology*, **189**, 115–117.
- Schneider, C., Laizé, C.L.R., Acreman, M.C. and Florke, M. 2013. How will climate change modify river flow regimes in Europe? *Hydrology and Earth System Sciences*, **17**, 325–339.
- Sharp, Z. 2017. *Principles of stable isotope geochemistry, 2nd edition*. University of New Mexico. DOI : [10.5072/FK2GB24S9F](https://doi.org/10.5072/FK2GB24S9F).
- Stewart, M.K. 1975. Stable isotope fractionation due to evaporation and isotopic exchange of falling waterdrops: Applications to atmospheric processes and evaporation of lakes. *Journal of Geophysical Research*, **80**, 1133–1146.
- Trenberth, K.E. 1999. Atmospheric moisture recycling: Role of advection and local evaporation. *Journal of Climate*, **12**, 1368–1381.

- Uemura, R., Matsui, Y., Yoshimura, K., Motoyama, H. and Yoshida, N. 2008. Evidence of deuterium excess in water vapor as an indicator of ocean surface conditions. *Journal of Geophysical Research*, **113**, D19114, doi:10.1029/2008JD010209.
- Vimeux, F., Gallaire, R., Bony, S., Hoffmann, G., Chiang, J.C.H. 2005. What are the climate controls on δD in precipitation in the Zongo Valley (Bolivia)? Implications for the Illimani ice core interpretation. *Earth and Planetary Sciences*, **240**, 205–220.
- Wang, S., Zhang, M., Che, Y., Chen, F. and Qiang, F. 2016. Contribution of recycled moisture to precipitation in oases of arid central Asia: A stable isotope approach. *Water Resources Research*, **52**, 3246–3257.
- Wang, X. F. and Yakir, D. 2000. Using stable isotopes of water in evapotranspiration studies. *Hydrological Processes*, **14**, 1407–1421.
- Wypych, A., Bochenek, B. and Różycki, M. 2018. Atmospheric moisture content over Europe and the Northern Atlantic. *Atmosphere*, **9**, 18. Doi: 10.3390/atmos9010018.
- Yurtsever, Y. 1975. Worldwide survey of stable isotopes in precipitation: Reports section isotope hydrology. *International Atomic Energy Agency, Vienna*, 1–40.

Figure captions

Fig. 1. A – Geographic distribution of IAEA stations over Europe. Those stations have been used to calculate the $\delta^2\text{H}-\delta^{18}\text{O}$ slopes recorded at each station georeferenced by its latitude (ϕ) and longitude (λ). IAEA stations that are under the influence of the Mediterranean climate, i.e. those located around the Mediterranean Sea, were not taken into account to build the database. The background map is extracted from Google Earth®. The correspondence between numbers reported on the map and city names is listed as follows:

1 – Valentia, Ireland. 2 – Inchnadamph, U.K. 3 – Plouzané, France. 4 – Altnabreac, U.K. 5 – Wallingford, U.K. 6 – Keyworth, U.K. 7 – Dax, France. 8 – Cestas-Pierroton, France. 9 – Fleam Dyke, U.K. 10 – Campistrous, France. 11 – Orléans-La-Source, France. 12 – Braakman, Netherlands. 13 – De Kooy, Netherlands. 14 – Gilze-Rijen, Netherlands. 15 – Wieringerwerf, Netherlands. 16 – De Bilt, Netherlands. 17 – Liège, Belgium. 18 – Beek, Netherlands. 19 – Thonon-Les-Bains, France. 20 – Draix, France. 21 – Groningen, Netherlands. 22 – Lista, Norway. 23 – Emmerich, Germany. 24 – Trier, Germany. 25 – Weil Am Rhein, Germany. 26 – Bern, Switzerland. 27 – Belp, Switzerland. 28 – Meiringen, Switzerland. 29 – Karlsruhe, Germany. 30 – Cuwhaven, Germany. 31 – Bad Salzuflen, Germany. 32 – Locarno, Switzerland. 33 – Konstanz, Germany. 34 – Stuttgart, Germany. 35 – Wuerzburg, Germany. 36 – Braunschweig, Germany. 37 – Hohenpeissenberg, Germany. 38 – Garmisch-Partenkirchen, Germany. 39 – Neuherberg, Germany. 40 – Hof-Hohensaas, Germany. 41 – Regensburg, Germany. 42 – Taastrup, Denmark. 43 – Leipzig, Germany. 44 – Berlin, Germany. 45 – Klagenfurt Flughafen, Austria. 46 – Uhlirka, Czech Republic. 47 – Petzenkirchen, Austria. 48 – Graz, Austria. 49 – Vienna, Austria. 50 – Podersdorf, Austria. 51 – Liptovsky, Slovakia. 52 – Krakow, Poland. 53 – Naimakka, Sweden. 54 – Brest, Belarus. 55 – L'vov, Ukraine. 56 – Riga, Latvia. 57 – Espoo, Finland. 58 – Rovaniemi, Finland. 59 – Minsk, Belarus. 60 – St. Petersburg, Russia. 61 – Odessa,

Ukraine. 62 – Kandalaska, Russia. 63 – Murmansk, Russia. 64 – Kalinin, Russia. 65 – Kursk, Russia. 66 – Rjazan, Russia. 67 – Vologda, Russia. 68 – Arkhangelsk, Russia. 69 – Tambov, Russia. 70 – Gor'kij, Russia. 71 – Astrakhan, Russia. 72 – Kirov, Russia. 73 – Perm, Russia. 74 – Pechora, Russia. 86 – La Coruna, Spain. 91 – Ponferrada, Spain. 93 – Leon/Virgen, Spain. 98 – Santander, Spain.

B – Map of the European climate zones after Schneider *et al.* (2013). Empty arrow: direction of Arctic winds; Black arrow: direction of westerlies. Climatic zones: red = Mediterranean; bottle green = Temperate oceanic; green = temperate transitional; light green = temperate continental; pink = boreal; blue = polar.

Fig. 2. Monthly weighted $\delta^2\text{H}$ reported against the monthly weighted $\delta^{18}\text{O}$ of precipitation in Berlin for the period comprised between years 1978 and 2001. Linear regression of data for the twelve months allows the following equation to be computed: $\delta^2\text{H} = 7.97(\pm 0.37)\delta^{18}\text{O} + 6.46(\pm 3.14)$ with a $R^2 = 0.98$.

Fig. 3. A – Hela index K of continentality (see equation (2) for a definition) reported against the longitude ϕ of the considered IAEA stations.

B – Mean annual temperature range T_A (= difference between the coldest and the month of the year) reported against the longitude ϕ of the considered IAEA stations.

C – Latitude λ (in $^\circ$) of the considered IAEA stations reported against their longitude ϕ (in $^\circ$).

Fig. 4. A – Slope S of the MWL recorded at each IAEA station as a function of their longitude ϕ . Two outliers were identified by the linear regression procedure that are the stations located in the cities of Riga, Latvia, and St. Petersburg, Russia. The station located at Odessa, Ukraine, has also been removed because of the large standard deviation ($SD = 1.63$, $R^2 = 0.77$) associated with the slope value.

B – Slope S of the MWL recorded at each IAEA station as a function of the decimal logarithm of their longitude ($\phi + 15$). The value of 15 was arbitrary chosen to make all the longitude values positive. This slope ranges from about 6 to 9 after the removal of three stations (Odessa, Ukraine; Riga, Latvia and St. Petersburg, Russia) that display quite large standard deviations around the mean value, including two outliers (Riga and St. Petersburg).

Fig. 5. Slopes S of the MWL calculated as a function of temperature T ($^{\circ}\text{C}$) on the basis of the experimentally-determined oxygen isotope fractionation factors α between liquid water (l) and water vapour (v) (green curves) and between water ice (i) and water vapour (v) (purple curve). Plain green curve was computed by combining equations (13) and (14) determined by Majoube (1971); dotted green curve was computed by combining equations (15) and (16) determined by Horita & Wesolowski (1994); purple curve was computed by combining equations (17) and (18) determined by Majoube (1970) and Merlivat & Nief (1967).

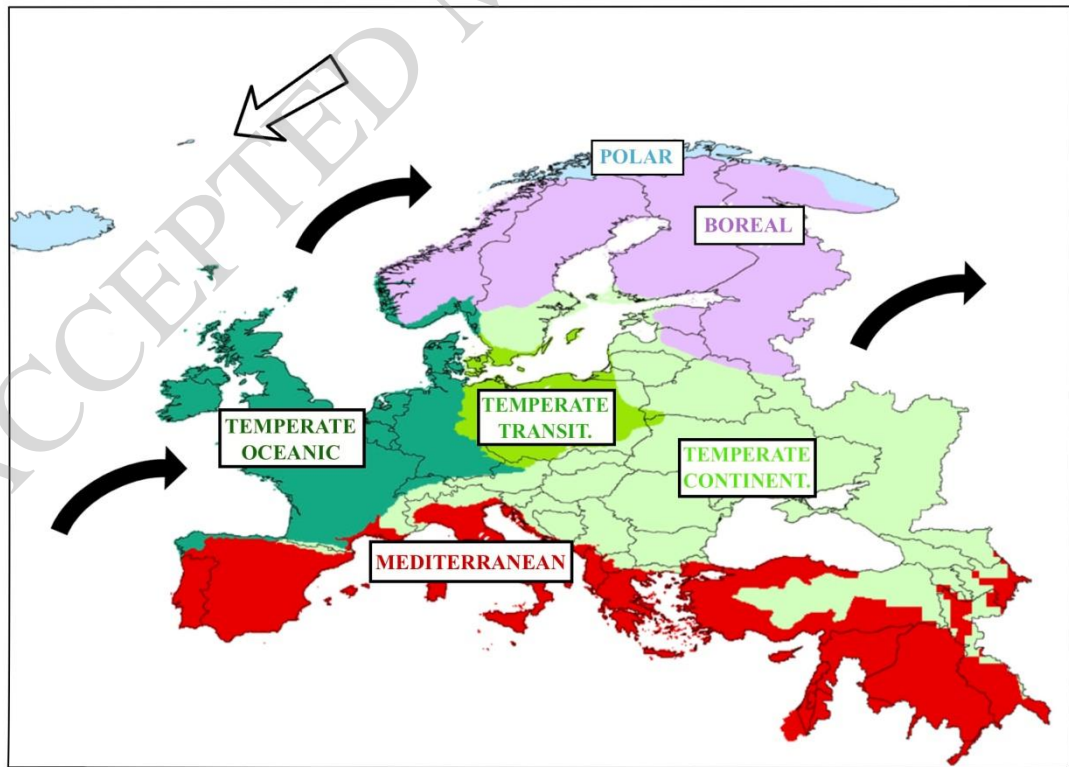
Supplementary Fig. 1. Weighted $\delta^2\text{H}$ reported against the weighted $\delta^{18}\text{O}$ of precipitation in Europe (stations located around the Mediterranean Basin have been excluded from the IAEA/WMO database. Linear regression of data allows the following equation to be computed: $\delta^2\text{H} = 8.07(\pm 0.13)\delta^{18}\text{O} + 9.62(\pm 1.21)$ with a $R^2 = 0.98$.

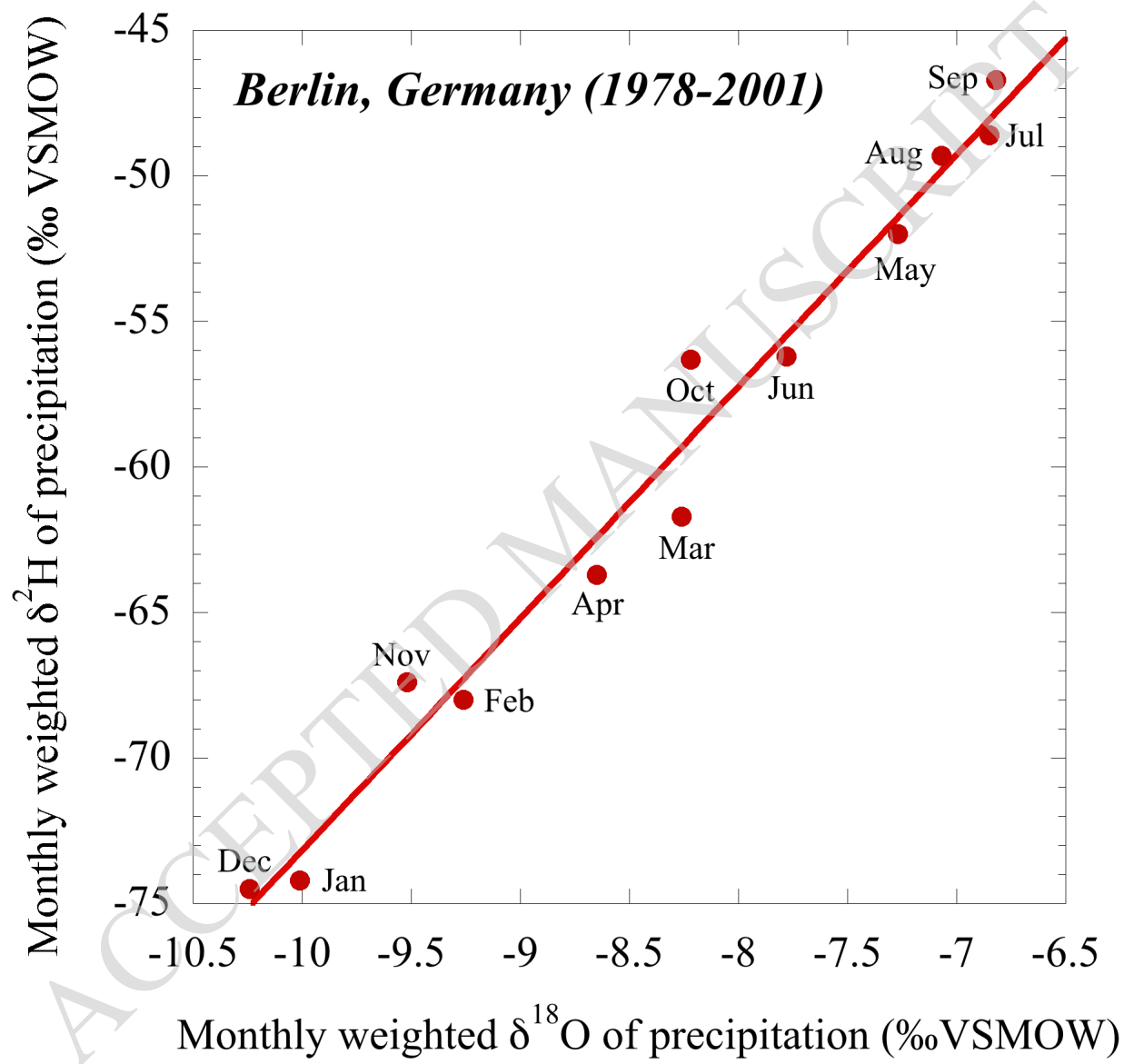
Supplementary Fig. 2. Frequency histogram of the coefficients of determination (R^2) associated with the slopes of the Meteoric Water Line (MWL) recorded at each IAEA station. The lowest R^2 values correspond to the cities of Wieringerwerf, Netherlands and Odessa, Ukraine ($R^2 \approx 0.77$), Riga, Latvia ($R^2 \approx 0.83$) and De Kooy, Netherlands ($R^2 \approx 0.89$).

A)

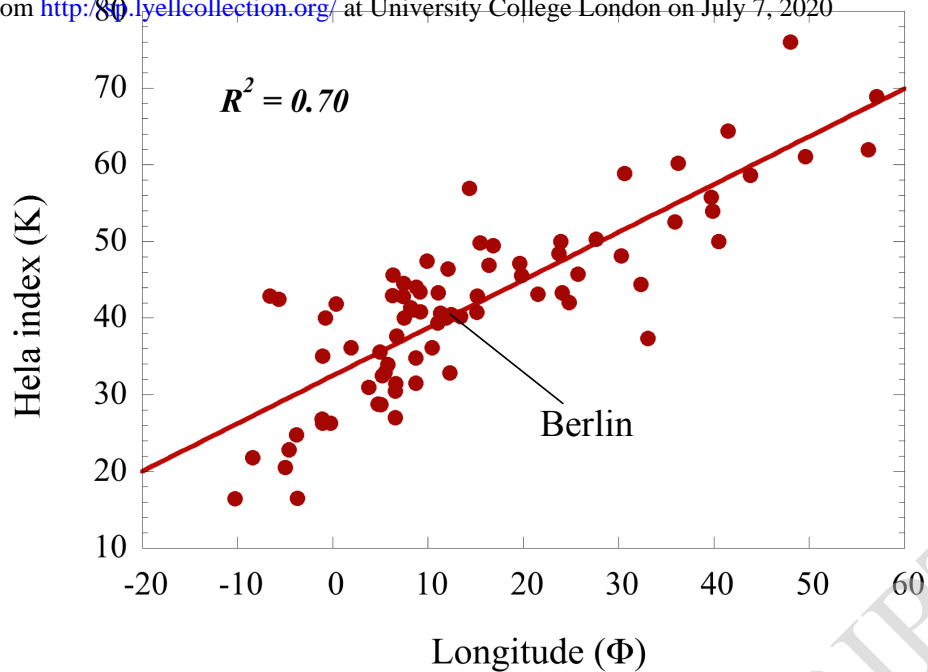


B)

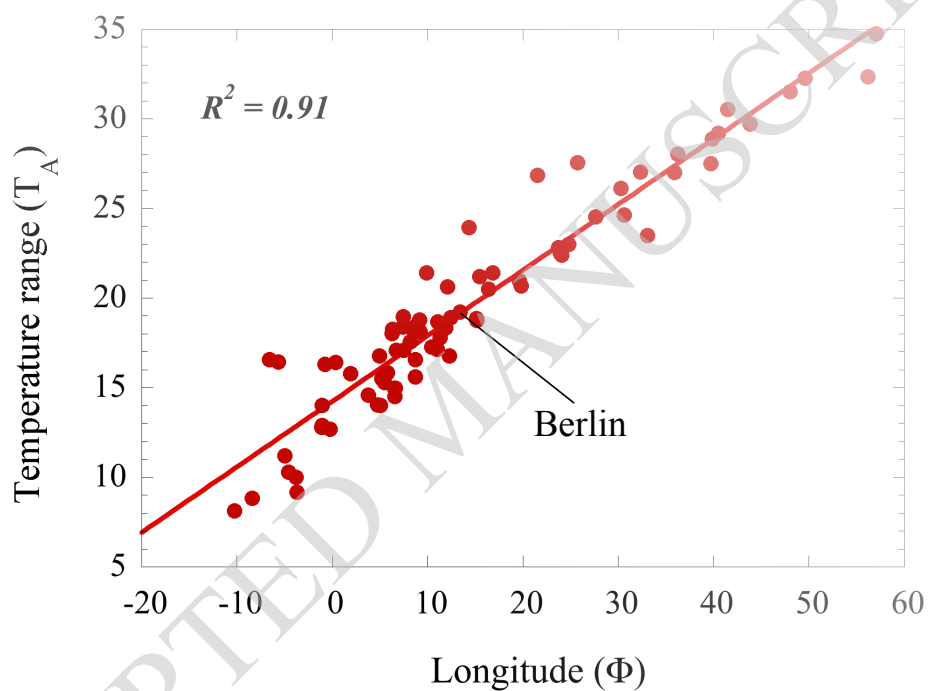




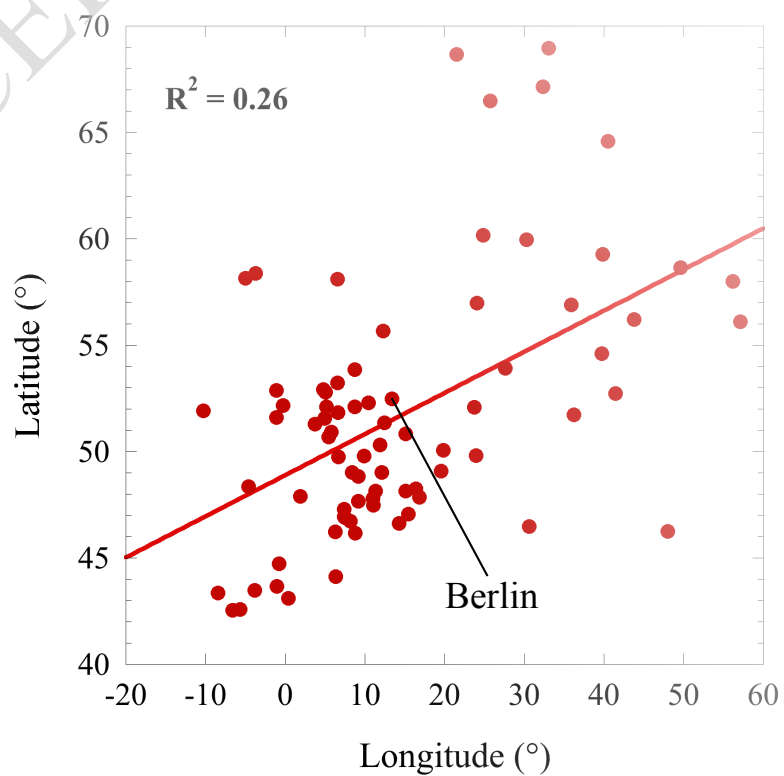
A)



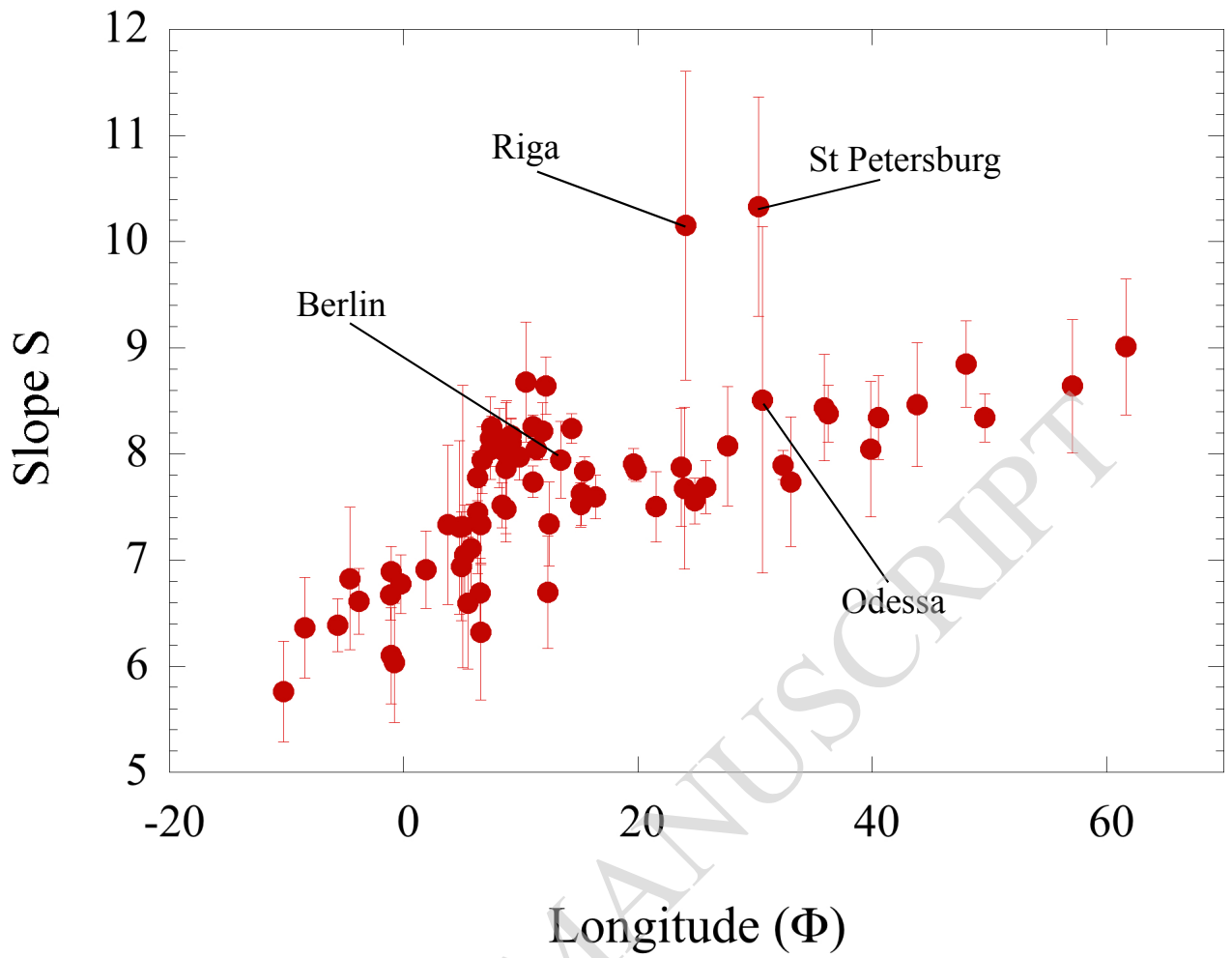
B)



C)



A)



B)

